NASA Technical Memorandum 102336

Heat Transfer to Throat Tubes in a Square-Chambered Rocket Engine at the NASA Lewis Research Center

James A. Nesbitt and William J. Brindley
Lewis Research Center
Cleveland, Ohio

October 1989

NASA

HEAT TRANSFER TO THROAT TUBES IN A SQUARE-CHAMBERED ROCKET ENGINE AT THE NASA LEWIS RESEARCH CENTER

James A. Nesbitt and William J. Brindley
National Aeronautics and Space Administration
Lewis Research Center
Cleveland, Ohio 44135

SUMMARY

A gaseous H_2/O_2 rocket engine was constructed at the NASA Lewis Research Center to provide a high heat flux source representative of the heat flux to the blades in the high-pressure fuel turbopump (HPFTP) during start-up of the space shuttle main engines. The high heat flux source was required to evaluate the durability of thermal barrier coatings being investigated for use on these blades.

The purpose of the present work was to evaluate the heat transfer, and specifically, the heat flux to tubes located at the throat of the test rocket engine and to compare this heat flux with the heat flux to the blades in the HPFTP during engine start-up. This purpose was accomplished by measuring gas temperatures, pressures and heat transfer coefficients in the test rocket engine. Near-surface metal temperatures below thin thermal barrier coatings were also measured at various angular orientations around the throat tube to indicate the angular dependence of the heat transfer coefficients.

A finite-difference model for a throat tube was developed and a thermal analysis was performed using the measured gas temperatures and the derived heat transfer coefficients to predict metal temperatures in the tube. Near-surface metal temperatures of an uncoated throat tube were measured at the stagnation point and showed good agreement with temperatures predicted by the thermal model.

The maximum heat flux to the throat tube was calculated and compared to that predicted for the leading edge of an HPFTP blade. It is shown that the heat flux to an uncooled throat tube is slightly greater than the heat flux to an HPFTP blade during engine start-up.

INTRODUCTION

The three variable thrust, liquid hydrogen-fueled main engines powering the space shuttle orbiters are the most advanced rocket engines designed and flown to date. However, several components suffer from premature replacement far short of the design life due to the severe operating environment within the engine. Hence, the pursuit of improved durability is an ongoing task for several space shuttle main engine (SSME) components. The first stage blades within the high-pressure fuel turbopump (HPFTP) have received much of this attention regarding improved durability.

The main engines utilize a staged combustion power cycle with hydrogen being only partially burned at low mixture levels (hydrogen-rich) in preburners.

The HPFTP consists of a preburner, a two-stage axial turbine and a three-stage centrifugal pump. The preburner operates at a pressure of approximately 38.3 MPa (5600 psi) and an oxidizer to fuel mass ratio near 1 (O/F = 1)[1] which produces a hot-gas temperature of approximately 870 °C (1600 °F) (ref. 1). The hydrogen-rich steam from this preburner drives the turbine, thereby powering the pump. This pump circulates liquid hydrogen which, in addition to being used as the fuel, is utilized as a coolant for the main combustion chamber and nozzle. The hydrogen-rich steam exiting the turbine is injected into the main combustion chamber with additional hydrogen and oxygen.

Upon ignition, the gas temperatures in the fuel preburner undergo two thermal transients within the first 2 sec before rising to the steady-state value near 870 °C (1600 °F) (ref. 2). The gas temperature during the first thermal excursion reaches approximately 1750 °C while the temperature during the second thermal excursion reaches only 750 °C (fig. 1(a)). These thermal transients during engine start-up are believed to contribute to the formation and/or propagation of cracks observed in the HPFTP blades. The temperature of a first-stage HPFTP blade during a typical mission cycle has been predicted using a finite element thermal model (ref. 2). Metal temperatures predicted by this model for the leading edge near the blade tip during the two thermal transients at engine start-up are also shown in figure 1(a). The predicted heat transfer coefficient (h_c) at this location (ref. 3) is dependent on the gas pressure, temperature and rotational velocity of the turbine and therefore changes with time as shown in figure 1(b) for the period of engine start-up. Fortunately, h_c during the first thermal transient is only a fraction of the steady-state value of 383 kW/m^2 K so that the surface temperatures of the blades remain below the melting point.

The use of plasma-sprayed thermal barrier coatings (TBC's) was proposed during early development of the SSME when the severe thermal transients in the HPFTP, as well as cracking in the blades, became apparent (ref. 4). However, the thermal transients also caused spallation and loss of the outer ceramic layer of the TBC. Consequently, the blades are currently only coated with a thin Ni-Cr-Al-Y metallic layer which provides minimal thermal protection. Advances throughout the 1980's in the development of TBC's for aero gas turbine engines prompted a reexamination of their potential for damping the thermal shock to the HPFTP blades. A research program was initiated at the NASA Lewis Research Center to evaluate a variety of vendor coatings as well as TBC's developed at NASA Lewis. A hydrogen-oxygen test rocket (designated TSTR for Thermal Shock Test Rocket) was designed and developed to test and evaluate the TBC's which were applied to directionally solidified (DS) Mar-M246+Hf[2] rods and tubes. This substrate material is the same as that currently used for the HPFTP blades. The test specimens were located at the throat of the rocket engine with the cylindrical axis perpendicular to the gas flow. The rocket engine is capable of producing gas temperatures in the range of 1100 to 3100 °C (2000 to 5600 °F) at pressures up to 4.1 MPa (600 psi).

The purpose of the present work was to evaluate the heat transfer, and specifically the heat flux, to tubes located at the throat of the rocket engine and to compare this heat flux with the heat flux to the blades in the HPFTP

---

[1]For 109 percent full-power level.

[2]The composition of DS Mar-M246+Hf is Ni-10Co-9Cr-10W-5.5Al-2.5Mo-1.5Ta-1.5Ti-0.15C-0.015B-0.05Zr-1.75Hf wt %.

during engine start-up. This purpose was accomplished by measuring gas temperatures and pressures in the throat region of the rocket engine and heat transfer coefficients for the tubes located at the throat. Near-surface metal temperatures below thin thermal barrier coatings were also measured at various angular orientations around the throat tube to indicate the angular dependence of the heat transfer coefficients. A finite-difference model for a throat tube was developed and a thermal analysis was performed using the measured gas temperatures and the calculated heat transfer coefficients to predict metal temperatures in the tube. Near-surface metal temperatures of a throat tube were measured at the stagnation point facing the injector and used to validate measured gas temperatures and heat transfer coefficients and to verify the predictive capability of the thermal model.

The maximum heat flux to an uncoated throat tube in the TSTR was calculated and compared to that predicted for the leading edge of an HPFTP blade. It was found that the heat flux to an uncoated throat tube is slightly greater than the predicted heat flux to an HPFTP blade during engine start-up. A thermal analysis of the heat transfer to thermal barrier coated tubes and rods tested in the TSTR and the potential benefit of applying TBC's to HPFTP blades is discussed in a companion paper (ref. 5). Durability testing of TBC's in the test rocket engine is discussed elsewhere (ref. 6).

EXPERIMENTAL PROCEDURE AND RESULTS

Rocket Engine Operation

A schematic of the TSTR developed at NASA Lewis and the copper specimen holder is shown in figure 2(a) with the actual injector, water-cooled combustion chamber and copper specimen holder shown in figure 2(b). A view of the test rocket while firing, showing the hot gas exiting the engine and entering the exhaust pipe, is shown in figure 2(c). Five 0.953 cm (0.375 in.) tubes or rods are held in the copper specimen holder such that all gas flow is perpendicular to the cylindrical axis. The hot gas exiting the combustion chamber is constricted by the presence of the tubes located at the throat of the rocket engine. High pressure in the combustion chamber results in Mach 1 exhaust gas velocities slightly upstream from the throat plane (the plane passing through the cylindrical axis of the tubes with the smallest cross-sectional area in the throat). The area blockage ratio for the engine, given as W/(W-D) (fig. 2(a)), is equal to 2.875 giving an area reduction (inverse of the area blockage ratio) at the throat of 0.348. Only three of the five specimens are fully exposed in the gas flow (tubes in test positions 2 to 4, fig. 2(a)). Preliminary test firings of the rocket engine indicated significant temperature differences between the three center test positions; position 4 was hottest while position 3 exhibited a cool region midway along the length of the tube most likely due to the large igniter orifice located in the center of the injector (fig. 2(b)). In an effort to maintain temperature uniformity between tests of different TBC's, all testing of thermal barrier coated tubes and rods was performed with test specimens in position 2. Hence, all heat transfer measurements and gas temperatures were measured at or near this position.

Most gas temperature measurements were made at an indicated oxidizer to fuel ratio of 1 (O/F = 1). This O/F ratio resulted in a hydrogen-rich environment similar to that in the HPFTP. The O/F ratio was calculated from flow rates into the engine which are controlled by sonic flow orifices. The

engine could not be consistently ignited at lower O/F ratios due to the excessively-rich fuel mixture. Standard operation of the engine involved opening the O_2 valve 0.1 sec before opening the H_2 valve which generally ensured engine ignition at this low O/F ratio. Generally the test duration was 1.2 or 1.3 sec but was increased to 3.5 sec to reach steady-state conditions when using a water-cooled instrumented tube. At the end of the test, the O_2 valve was closed 0.3 sec prior to the closing of the H_2 valve which resulted in a short H_2 purge. As either the O_2 or the H_2 valve was closed, each line was purged by gaseous N_2 which resulted in N_2 purging the specimens to room temperature. The pressure in the chamber of the rocket engine was maintained at approximately 2.07 MPa (300 psi) and generally varied from day to day by less than 3 percent. Repeatability of the chamber pressure is indicated in figure 3 where the chamber pressure for five different tests measured over a 5 month period is shown.

Gas Temperature Measurements

Five different thermocouple (tc) configurations were used to measure gas temperatures near test position 2. The different tc designs, including butt-welded, shielded, wedge-type, and a sonic orifice probe, are shown in figure 4. All tc assemblies used either Type R or B Pt/Pt-Rh wire running through alumina or magnesia sheathing which was encased in 0.318 cm (0.125 in.) o.d. molybdenum (Mo) tubes. The ceramic sheathing material without the protection of the Mo tube fractured during testing due to the thermal shock and/or gas forces. Wire diameters varied from 0.0254 to 0.0635 cm (0.010 to 0.025 in.). The Type B wire was chosen because of its greater mechanical strength over Type R wire; however, no improvement in the durability of the tc's with Type B wire was observed. Thermocouple shields (fig. 4(d)) were fabricated from Mo and welded to the Mo tubes encasing the ceramic sheathing. Likewise, Mo was also used for most parts of the sonic probe assembly (fig. 4(e)). The Mo parts of the sonic probe assembly were joined by gas tungsten arc welding in an inert welding chamber.

The sonic probe assembly required calibration to position the thermocouple bead at the plane of Mach 1 gas velocity within the sonic orifice and to determine the temperature correction for the instrument. Both calibrations were performed at room temperature as described in references 7 and 8. The relationship between the total temperature and that indicated by the sonic probe is given by:

$$T_t = \alpha T_i$$

where α is a variable which is dependent on the specific heat ratio of the gas and an empirically determined recovery factor unique to the sonic probe. The value of α at room temperature was 1.08 and at 1300 °C the value was calculated as 1.05. Specific dimensions of the assemblies, wire diameters, and wire type are given in table I. All tc assemblies generally failed after only one or two tests by fracture of the tc wire at or near the location where the wire exited the ceramic sheathing.

Gas temperatures were measured at four locations along the length of the tube from the midpoint to the copper wall and at six angular positions around the tube near the midpoint as indicated in figure 5. These locations will be referred to as tc position 1A, 2A, 3A, etc. giving the angular position

around the tube (positions 1 to 6) and along the tube axis (positions A to D). Temperatures at tc positions 1A and 4A were measured at the throat plane with butt-welded tc assemblies by inserting the tc's through holes drilled through the top of the copper specimen holder and through the upper tube (position 1) for tc position 1A and through the tubes at positions 1 and 2 for tc position 4A. The tc wire for the measurements at these two positions was oriented perpendicular to the gas flow. Gas temperatures along the tube axis (positions A to D) were measured at positions 2 and 3 with shielded wedge tc's and at position 5 with the sonic probe oriented such that the inlet hole was facing the injector. Measurements on the exhaust side of the test tube (position 6) were made with wedge tc's. Corrections (recovery, radiation, etc.) for the butt-welded and shielded tc's are discussed in the Analysis and Discussion section.

Gas temperatures measured at tc positions 1A and 2A are shown in figure 6(a), measurements made at tc positions 3A to 5A are shown in figure 6(b), and temperatures measured on the exhaust side of the test tube at tc position 6A are shown in figure 6(c). In general, temperatures measured at positions 1A, 2A and 6A showed the same general pattern of a maximum temperature within the first 0.2 sec of the test followed by a somewhat more uniform and constant steady-state temperature. As expected, temperatures measured with the shielded wedge tc's rose more slowly than those of the butt-welded tc's due to the larger thermal mass of the shield (see the inset in fig. 6(a)) although the steady-state temperatures measured with the butt-welded tc's at position 1A were also consistently higher than the temperatures measured at position 2A with the shielded wedge tc's. However, the difference in the individual temperature measurements at position 1A with the butt-welded tc's (50 to 100 °C) suggests that the difference between butt-welded and shielded tc's, after the initial temperature rise, may not be significant. Although significant temperature differences were observed, some measurements made on the same day exhibited very good repeatability (note the closely-grouped measurements made with five different butt-welded tc's at tc position 1A shown in the inset to fig. 6(a)). Several measurements made at tc positions 3A to 5A show a maximum in temperature near the beginning of the test similar to that at positions 1A, 2A and 6A; however, this behavior was not consistent among all measurements at these locations. In addition, the measured temperatures at positions 3A to 5A show a significant variation of up to approximately 200 °C which could not be correlated with or attributed to the different types of tc assemblies. Furthermore, temperatures measured at these positions (3A to 5A) are, on average, 200 °C greater than those measured at tc positions 1A and 2A. Similarly, the average steady-state temperatures measured at positions 1A and 2A are approximately 50 °C above the average temperatures measured at position 6A. The dashed lines in figures 6(a) to (c), indicate representative gas temperatures for positions 1A and 2A, for positions 3A to 5A, and for position 6A, and are discussed further in the following section.

A significant temperature reduction was measured in a direction parallel to the tube axis from the midpoint (tc position A) to the rocket chamber wall (position D). Temperature measurements made at locations tc positions 2B, 6C and 2D are shown in figure 7. Gas temperatures were also measured at O/F ratios slightly greater than one. Figure 8 shows gas temperatures measured at tc position 1A for O/F = 1.1 and 1.19 and the dashed line indicating the representative temperatures at this position at an O/F = 1.0. The steady-state gas temperatures increased approximately 140 °C for a 10 percent increase in the O/F ratio.

Heat Transfer Measurements

Instrumented stainless steel tube. - Heat transfer coefficients (h_c) were measured with an instrumented, water-cooled stainless steel tube. A schematic cross section of the instrumented tube is shown in figure 9. The 0.953 cm o.d., 0.648 cm i.d. (0.375 in. o.d., 0.255 in. i.d.) tube was initially cut longitudinally into two halves. Channels 0.038 cm (0.015 in.) in depth by 0.056 cm (0.022 in.) in width were cut on the inside and outside of the tube wall and individually sheathed thermocouples, 0.0254 cm (0.010 in.) diameter sheath with 0.0065 cm (0.003 in.) diameter wire, were placed in the channels and the beads welded to the bottom of the channel. The channels were covered with a 0.013 cm (0.005 in.) Inconel 600 sheet which was welded in place to seal the channel from the hot gas (outside) and water (inside). Large slots were also cut into the inner tube wall and filled with high-temperature ceramic cement to reduce tangential heat flow within the tube wall. Identical channels were cut in both halves of the tube to allow wall temperatures to be measured at two locations 180° apart. The two halves were welded together and the weld seam was smoothed to match the contour of the tube.

The instrumented tube was placed in a special copper specimen holder which permitted the tube to be water cooled for an extended test of 3.5 sec duration. The difference in temperature across the wall, along with the thermal conductivity of the stainless steel and the previously-measured gas temperature, allowed calculation of h_c at a particular angular orientation. Temperature differences across the tube wall were successfully measured only at 90° and 180° from the stagnation point. Representative temperatures near the inner and outer wall surface are shown in figure 10. It is believed that the unsuccessful tests at other orientations were due to thermocouple bead detachment from the bottom of the channel resulting in significantly lower measured temperatures. Two instrumented tubes were fabricated; however, failure in the supply of cooling water during the first test resulted in the destruction of one of the tubes after approximately 1 sec.

Angular dependence of the gas pressure around tubes. - The angular dependence of the gas pressure around the test tube was measured to allow comparison to other studies of the pressure distribution around throat tubes in square-chambered rocket engines (refs. 9 and 10). Gas pressures around the test tube were measured by rotating a single tube with four 0.063 cm (0.025 in.) pressure taps spaced 90° apart. These pressures, normalized to the chamber pressure, are shown in figure 11.

Surface Temperature Measurements of Bare and TBC Coated DS Mar-M246+Hf Tube

A DS Mar-M246+Hf tube was instrumented to measure near-surface metal temperatures which were later used to evaluate the usefulness of the measured gas temperatures and derived heat transfer coefficients by comparison to predicted metal temperatures. The tube was instrumented by placing a thermocouple 0.038 cm (0.015 in.) below the surface in an identical manner as that for the water-cooled stainless steel tube (fig. 9). The tube was tested for a 1.3 sec with the thermocouple channel facing the injector at an indicated O/F ratio of 1. The measured near-surface temperature is shown in figure 12. Localized

surface melting of the Mar-M246+Hf tube was observed at approximately 0.5 to 1.0 cm from the midpoint of the tube indicating the nonuniform temperature distribution at the rocket engine throat. The maximum temperature shown in figure 12 (1310 °C) is in good agreement with the melting point of Mar-M246 alloys (1316 to 1343 °C) (ref. 11). The surface melting was avoided on other Mar-M246+Hf tubes by applying a TBC. The rapid temperature decrease between 6.3 and 6.6 sec (see inset) occurs during purging with H_2 and the more gradual cooling after 6.6 sec occurs during purging with N_2. The rapid cooling by the H_2 gas indicates the beneficial thermal properties of H_2 gas when it is used as a coolant.

Near-surface metal temperatures were measured at various angular orientations on four Mar-M246+Hf tubes coated with a plasma-sprayed ZrO_2-Y_2O_3 TBC. The TBC gave sufficient thermal protection to keep the surface metal temperature below the melting point of the alloy allowing measurement of metal temperatures at different angular orientations. These measurements were then used to indicate the angular dependence of the heat transfer coefficient. The instrumented tubes were first coated with a thin, plasma-sprayed 0.025 to 0.050 cm (0.001 to 0.002 in.) Ni-Cr-Al-Y bond coat layer. The ceramic top coat was plasma sprayed to thicknesses ranging from 0.011 to 0.0024 cm (0.0045 to 0.0095 in.). Details of the plasma spraying process are given in reference 5. Temperatures were measured at different angles from the stagnation point by rotating the tubes. Test duration was 1.2 sec at an indicated O/F = 1. Some of the coated tubes were tested in the as-sprayed condition, after which the surface was smoothed by sanding with SiC paper and the coatings were retested to evaluate the effect of surface roughness. The surface roughness of the as-sprayed coatings was approximately 9.6 μm (377 μin.) (RA) and following sanding the roughness was reduced to an average value of 4.1 μm (163 μin.) (RA). The coating thickness following sanding was only slightly less than that prior to sanding; the sanding process appeared to mainly reduce peaks in the surface coating morphology. The near-surface metal temperatures at 0°, ±90°, and 180° for a 0.024 cm (0.0095 in.) ceramic coating are shown in figure 13(a), temperatures at 0°, 90°, and 180° for a 0.011 cm (0.0045 in.) ceramic coating are shown in figure 13(b), temperatures at 0° before and after sanding for a 0.0127 cm (0.005 in.) ceramic coating are shown in figure 13(c), and temperatures at 0° and ±45° for the same sanded ceramic coating are shown in figure 13(d). It is apparent from figure 13(c) that the roughness of the surface has little effect (within the uncertainty of the gas temperature) on the heat transfer to the tube.

An attempt was made to determine average heat transfer coefficients by flowing water through a copper throat tube and measuring inlet and outlet water temperatures. However, due to the large decrease in gas temperature measured along the length of test tube (fig. 7), results from this test were considered of little value and will not be discussed.

ANALYSIS AND DISCUSSION

Gas Temperature Measurements

Butt-welded thermocouples. - Thermal model: A thermal model for the butt-welded tc's located at the throat plane (positions 1A and 4A) was developed to determine the necessary recovery, conduction and radiation corrections to

the measured tc temperatures.[3] The SINDA thermal analyzer (ref. 12), utilizing finite-difference techniques, was used to solve the necessary thermal equations. A schematic of the thermal model is shown in figure 14. Both 0.025 and 0.050 cm (0.010 and 0.020 in.) diameter, Types B and R tc's were modelled. The length of exposed wire was varied from 0.18 to 0.36 cm (0.07 to 0.14 in.) to match the actual tc dimensions (table I). The length of tc wire within the ceramic insulator was approximately 2.5 cm (1.00 in.). Heat flux to the exposed thermocouple wire was modelled as a cylinder in crossflow using average heat transfer coefficients. These coefficients are dependent on the wire diameter and the hot gas properties according to the relationship given as (ref. 13):

$$Nu = \frac{h_{c,avg} D_o}{k_f} = C\left(\frac{V D_o}{\nu_f}\right)^n \qquad (1)$$

where Nu is the Nusselt number, $h_{c,avg}$ is the average heat transfer coefficient, D_o is the wire diameter, V is the gas velocity, and k_f and ν_f are the thermal conductivity and kinematic viscosity of the gas. The parameters C and n are dependent on the Reynolds number, Re, and have the values 0.174 and 0.618, respectively, for $4000 < Re < 40\,000$ (ref. 13). The fluid properties were calculated for an H_2-H_2O mixture at temperatures of 1174 and 1338 °C[4] (appendix A) and are given in table II along with other parameters used in equation (1). As the pressure in the chamber increased at the beginning of the run (fig. 3), $h_{c,avg}$ was scaled with the 0.8 power of the normalized chamber pressure ($P_{chamber}/P°$ where $P° = 2.07$ MPa) to reflect the pressure dependence of the heat transfer coefficient assuming turbulent heat transfer. Temperature-dependent thermal conductivities and emissivities for the Pt and Pt-Rh tc wires were utilized within the thermal model. The temperature dependency of the thermal conductivity for the Pt-6Rh, Pt-13Rh, and Pt-30Rh alloys was derived by interpolating between data for Pt and Pt-40Rh alloys given in reference 14. The temperature dependence of the total emissivity of Pt-Rh wire was taken from the suggested curve given in reference 15 which varies from approximately 0.1 at 500 °C to 0.2 at 1530 °C. The wire was assumed to radiate to room temperature in order to determine the maximum radiation correction. The density and heat capacity of each alloy, necessary to calculate the thermal capacitance of each finite-difference node, were taken from reference 16.

A measured thermocouple temperature lags the actual gas temperature in a dynamic environment as a result of recovery, radiation, and conduction losses. The effect of these losses can be viewed separately with the thermal model of the butt-welded thermocouples. To view the effect of these losses, the dashed line shown in figure 6(a) was assumed as the actual gas temperature profile. (It will later be shown that this dashed line is representative of the actual

---

[3]Equilibrium thermodynamic calculations, to be discussed in a following section, predicted a negligible amount ($<1\times10^{-6}$ mol fraction) of atomic hydrogen or oxygen to be present. Hence, no temperature correction for atomic recombination on the Pt thermocouple wire was considered.

[4]The temperatures 1174 and 1338 °C were chosen to span the steady-state temperatures measured at tc positions 1A and 2A (fig. 6(a)) and tc positions 3A and 4A (fig. 6(b)).

gas temperature at tc positions 1A and 2A.) The lag in the predicted temperature response due to recovery losses and combined recovery and conduction losses for a 0.05 cm (0.020 in.) butt-welded thermocouple is shown in figure 15(a). The effect of the radiation correction on the predicted thermocouple temperature was less than 1 °C and has not been shown. It is apparent from this figure that conduction losses down the tc leads are more significant than recovery corrections in predicting the response of the thermocouple. After the maximum temperature is reached in approximately 0.2 sec, the predicted thermocouple temperature and the gas temperature are essentially indistinguishable. The effect of the wire diameter on the predicted thermocouple temperature after correcting for recovery, conduction and radiation losses is shown in figure 15(b). Again, there is little difference in the predicted thermocouple temperature and the gas temperature after the maximum temperature has been reached. Figures 15(a) and (b) indicate that the measured thermocouple temperatures for the butt-welded tc's are very close to the actual gas temperature.

The predicted temperature in the exposed wire and along the insulated tc leads at the maximum tc temperature (after 0.1 sec) is shown in figure 15(c). It is apparent that there is little temperature rise in the wire at approximately 1 cm from the tc bead. Even after 1.2 sec, the nodes furthest from the tc bead (0.8 in.) were predicted to have risen only 2 to 3 °C. Hence, the length of the wire leads in the tc model were sufficiently long so as to represent the actual tc leads. Using the same gas temperature profile, there was no significant difference in the predicted thermocouple response between the Types B and R tc wire, nor was there a significant difference in the temperatures (<5 °C) along the wire leads for the different tc alloy combinations (i.e., Pt and Pt-13Rh). Hence, it is not necessary to model separately the different tc wire types (Type R or B) or to model both tc leads of different alloy composition for the time and temperature conditions examined in this study due to the similarity in the thermal conductivity, density and specific heat of the Pt alloys in Types R and B tc's.

Derived gas temperature profiles: Gas temperature profiles representative of actual gas temperature profiles were derived by matching predicted thermocouple temperatures, corrected for recovery, radiation and conduction losses, with the measured thermocouple temperatures shown in figure 6(a) (tc positions 1A and 2A) and figure 6(b) (tc positions 3A and 4A). The gas temperature profile producing a good match between predicted and measured tc temperatures was assumed to be representative of the actual gas temperature profile. However, as shown above, corrections to the measured tc temperatures are relatively small except for the initial temperature rise. Hence, the derived gas temperatures are approximately equal to the measured tc temperatures after approximately 0.1 sec and certainly within the uncertainty in the measured tc temperatures. The derived gas temperature profiles are shown as dashed lines in figure 6(a) (for tc positions 1A and 2A) and figure 6(b) (for tc positions 3A and 4A).

Shielded and wedge thermocouples. - Recovery and radiation corrections for the shielded tc's are given in reference 17. The recovery correction for a gas velocity of Mach 0.9 and 0.10 MPa (14.7 psi) pressure is less than 1 percent of the measured temperature. At the higher pressures used in the present study, this recovery correction would be even less. The radiation correction is relatively small because of the shield and amounts to approximately 9 °C for the shielded tc's used in this study. The recovery and radiation corrections

for the unshielded wedge tc's are also given in reference 17 and are greater than those for the shielded tc's. The radiation correction for an indicated tc temperature of approximately 1300 °C is 18 °C. However, since the unshielded wedge tc's were only used to measure temperatures at 180° from the stagnation point where the gas velocity was unknown, the magnitude of the recovery correction was uncertain. Because the scatter in the temperature measurements was significantly greater than the recovery and radiation corrections, these corrections were not applied to the temperatures measured by the shielded or wedge tc's shown in figure 6. Hence, the measured tc temperatures for both the butt-welded and the shielded tc's are very close to the actual gas temperature and certainly within the observed scatter in the temperature data.

The variations in measured gas temperatures at different locations around and along the test tube indicate that poor mixing of gases occurs in the rocket chamber. There was a significant variation in gas temperatures both vertically and horizontally which is most likely due to nonuniform oxygen or hydrogen gas injection. Some of the variation in the measured temperatures near the same location (i.e., tc positions 3A and 4A, fig. 6(b)) is believed to be due to inexact horizontal positioning in the direction for which a significant temperature variation was observed (fig. 7). In addition to the temperature decrease in a direction parallel to the tube axis, the localized surface melting of the uncoated Mar-M246+Hf tube, discussed above, indicates a hotter gas temperature 0.5 to 1.0 cm from the midpoint of the tube. The high temperatures measured at tc positions 1A and 2A for 0.2 sec at the beginning of the test (fig. 6(a)) are most probably due to the 0.1 sec lead in oxygen gas flow which results in an initially higher O/F ratio and consequent temperature spike.

Adiabatic equilibrium temperatures. - Equilibrium thermodynamic calculations assuming adiabatic conditions predict gas temperatures of 1002 °C for an O/F ratio of 1 and a chamber pressure of 2.07 MPa (300 psi) (ref. 18). The measured temperatures at tc position A at the midpoint of the tube axis were approximately 200 to 400 °C greater than this predicted temperature. It is believed that the actual O/F ratio near the midpoint of the tube at test position 2 was greater than the value calculated from input flow rates. Thermodynamic calculations predicting gas temperatures of 1200 to 1400 °C, as measured in the engine, indicate a localized O/F ratio of at least 1.2 to 1.4 near the midpoint of the tube.

Heat Transfer Coefficients

Heat transfer coefficient at 90° and 180°. - Heat transfer coefficients at 90° and 180° from the stagnation point were determined from temperature measurements at the inner and outer wall of the instrumented stainless steel tube (fig. 10). The thermal conductivity of the stainless steel at the respective wall temperature was taken from reference 14. Relatively low wall temperatures due to the water cooling precluded the need to correct for radiative heat losses from the tube surface. The steady-state heat flux through the wall was calculated as 8822 J/sec (8.37 Btu/sec) at 90° and 5702 J/sec (5.41 Btu/sec) at 180°. A gas temperature of 1210 °C (the steady-state gas temperature shown as a dashed line in fig. 6(a)) was used to determine h_c at 90°. A steady-state gas temperature of 1155 °C (see dashed line in fig. 6(c)) was used to determine h_c at 180°. The value for h_c determined at 90° and at 180° from

the stagnation point was 27.5 kW/m^2 K (4845 Btu/hr ft^2 °F) and 9.05 kW/m^2 K (1594 Btu/hr ft^2 °F), respectively.

Heat transfer coefficients at the stagnation point. - The heat transfer coefficient at the stagnation point ($h_{c,stag}$) can be predicted by assuming the presence of a laminar boundary layer as proposed by Squire for a cylinder in a free stream (ref. 13). However, to use Squire's equations in the present study, the Reynolds number must first be corrected for the effect of the channel blockage on the velocity distribution around the tube. Talmor (ref. 19) has reviewed various correction factors for the effect of blockage on the stagnation point heat transfer and suggests use of the correction by Robinson and Han (ref. 20). This correction factor is given as $1 + (D/W)^{1/2}$ where D is the outer diameter of the tube and W is the channel width normal to the longitudinal axis of the tube (fig. 2(a)) giving a channel blockage correction factor of 1.652 for the geometry of the rocket engine throat in this study. The gas velocity at the stagnation point of the tubes was calculated from the cross-sectional area of the throat at the stagnation point, the mass flow rates of H_2 and O_2 into the engine, and the density of the H_2-H_2O mixture at the two temperatures of 1174 and 1338 °C. The calculated gas velocity and Reynolds number (Re) associated with the 0.9525 cm tubes are shown in table III. The gas density and viscosity at these two temperatures are given in table II. The corrected Reynolds number for each temperature (table III), calculated as the product of Re and the channel blockage correction factor, have an average value of 128 000. Talmor (ref. 19) has correlated the ratio $Nu/(Pr)^{1/3}$ for the stagnation point of immersed cylinders with the corrected Reynolds number for various blockage ratios and turbulence intensities (Tu). For a corrected Re of 128 000, this correlation gives values of 400 to 570 for the ratio $Nu/(Pr)^{1/3}$ for Tu of 0 to 11 percent. For an average value of Pr = 0.586 and k_f = 0.508 W/m K (table II), the value of Nu at the stagnation point is 478 to 681 for Tu values of 0 to 11 percent yielding values of $h_{c,stag}$ of 25.5 to 36.3 kW/m^2 K (4500 to 6400 Btu/hr ft^2 °F). Values of the ratio $Nu/(Pr)^{1/3}$, Nu and h_c at Tu equal to 0 and 11 percent are given in table III.

Angular dependence of the heat transfer coefficient. - Talmor (ref. 9) measured the angular dependence of h_c for a single tube (2.54 cm o.d.) located at the throat of a square-chambered rocket engine and oriented in the same manner as the tubes in this study (tube axis horizontal and perpendicular to the gas flow). These measurements were made at various chamber pressures. Talmor also predicted the angular dependence of h_c based on the measured pressure distribution around the tube (fig. 11) assuming the presence of either a laminar or turbulent boundary layer around the tube. Excellent agreement was found between the measured and predicted heat transfer coefficients with the assumption of turbulent boundary layer formation. Talmor's results for the angular dependence of h_c normalized with the heat transfer coefficient at the stagnation point, $h_{c,stag}$, are shown in figure 16. Talmor also measured the pressure distribution around smaller throat tubes (0.953 cm o.d.) in a square-chambered rocket engine (fig. 11). The angular dependence of h_c was predicted from this pressure distribution assuming either laminar or turbulent boundary layer formation. Average heat transfer coefficients at different chamber pressures were also measured. Good agreement was observed between the measured average heat transfer coefficients and average heat transfer coefficients derived on the assumption of a turbulent boundary layer around most of the tube. The predicted angular dependence of h_c for the smaller throat tubes is also shown in figure 16.

The measured angular pressure dependence around the test tube in this study (fig. 11) is in good agreement with that measured by Talmor for the single cylinder (3.18 cm o.d.) (ref. 9) and the four cylinders (0.953 cm o.d.) (ref. 10) at the throat of the square-chambered rocket engine. In these two studies, Talmor reported flow separation from the tube at approximately 135° from the stagnation point where the pressure dropped to a minimum. Preliminary test firings of the TSTR with smooth ceramic-coated tubes resulted in the appearance of a dark deposit on the exhaust-side of the tubes (fig. 17). The deposit begins at approximately 133° from the stagnation point and appears to cover the region of flow separation. In addition, early testing of these tubes at higher gas temperatures resulted in melting of the ceramic which flowed from the injector side of the tube and separated from the tube at approximately 135° from the stagnation point, again indicating flow separation in agreement with the observations of Talmor on single and multiple throat tubes.

The ratio of h_c at 90° to that at 180° measured in this study (fig. 16) is in very good agreement with Talmor's findings for the same size tubes (0.953 cm o.d.). This agreement suggests that the value for h_c at the stagnation point of the tubes used in this study would be close to that at 90° (i.e., $h_{c,90} = 27.5$ kW/m^2 K). Indeed, the predicted values for $h_{c,stag}$ for $0 < Tu < 11$ percent is in very good agreement with the measured value at 90°, suggesting that the heat transfer coefficients in this study follow the angular dependence around the tubes measured by Talmor (ref. 9).

However, the near-surface temperatures measured between ±90° on the thermal barrier coated tubes (figs. 13(a), (b), and (d)) suggest that there is very little difference in h_c in this range in contrast to the results of Talmor. Surprisingly, temperatures measured at ±45° are almost identical to those at the stagnation point (fig. 13(d)) while temperatures measured at ±90° tend to be slightly less than those measured at the stagnation point (figs. 13(a) and (b)). The maximum in h_c between 0° and 90° found by Talmor is attributed to a turbulent boundary layer in this region. A laminar boundary layer in this region would cause the value of h_c to decrease from the stagnation point (refs. 9 and 13). Talmor predicted the transition from a laminar to turbulent boundary layer at chamber pressures of approximately 2.7 MPa (400 psi) with the 0.953 cm (0.375 in.) throat tubes. This transition would also be affected by the composition of the combustion gas, the level of turbulence in the approaching gas, and the length of the combustion chamber (the distance from the injector to the throat tubes). It is unclear in this study at what point the boundary layer becomes turbulent and what part turbulence in the combustion gas plays in this transition. The combustion chamber used in this study is relatively short (6 in.), similar to that used by Talmor, and would tend to encourage the transition from laminar to turbulent flow. However, the lower chamber pressure in this study (2.07 MPa (300 psi)) would tend to favor a laminar boundary layer delaying the transition to higher angles and higher velocities. Considering both the predicted value for $h_{c,stag}$ and the temperature data measured at different angles below the TBC's (fig. 13) suggests that $h_{c,stag}$ is slightly greater than the value measured at 90° (27.5 kW/m^2 K) and h_c decreases in a monotonic fashion from the stagnation point to a value around 27 kW/m^2 K at 90°. The angular dependence of h_c suggested by these results is shown in figure 16.

Modelling and Verification Test

A thermal model was developed to simulate heat transfer to, and conduction within, a throat tube in the TSTR. A schematic of the thermal model is indicated in figure 18. A 45° wedge facing the injector was modelled using 61 nodes, the outermost node being on the surface. Node spacing in the outer layers of the wedge was 0.000127 cm (0.0005 in.) and increased to 0.0051 cm (0.002 in.) near the inner wall. Two values for the heat transfer coefficient at the stagnation point were used, 27.5 kW/m^2 K representing the value measured at 90°, and 33 kW/m^2 K, a value 20 percent greater than that measured at 90°. Temperature-dependent radiative properties for the Mar-M246+Hf substrate were approximated from data for Ni-Cr-X alloys (ref. 15) and temperature dependent thermal properties (K, C_p) were taken from reference 21 and are given in appendix B. The inner wall of the tube was assumed to be insulated. Gas temperatures were those based on the results of the thermocouple models (see dashed lines in figs. 6(a) and (b)). The heat transfer coefficient used for the short (0.3 sec) H_2 purge at the end of the hot fire was 8.8 kW/m^2 K (1555 Btu/hr ft^2 °F) and that for the N_2 purge thereafter was 1.76 kW/m^2 K (311 Btu/hr ft^2 °F). Both heat transfer coefficients for the H_2 and N_2 purge were approximations based on the chamber pressures, flow rates and gas fluid properties (ref. 13).

Predicted temperatures at 0.038 cm (0.015 in.) below the surface of the tube for the two gas temperature profiles and h_c = 33 kW/m^2 K are shown in figure 12. The agreement between the predicted metal temperatures using the higher gas temperature profile (fig. 6(b)) and the measured metal temperatures is very good. The temperature differences are easily within the uncertainty in gas temperature. The maximum temperatures (time = 6.3 sec) for h_c = 27.5 kW/m^2 K were only 20 °C lower than those for h_c = 33 kW/m^2 K and indicate that the uncertainty in the value of h_c at the stagnation point does not prohibit the successful modelling of the thermal response of the tube within the known accuracy of the gas temperature. Hence, the good agreement for h_c = 33 kW/m^2 K justifies the use of this value for the heat transfer coefficient at the stagnation point and also indicates that the higher gas temperature profile (fig. 6(b)) is most appropriate for the stagnation point of the tubes.

Comparison of the Heat Flux in the TSTR and SSME-HPFTP

The heat flux to the first stage blades in the HPFTP was calculated for the two thermal transients which occur during engine start-up. The heat flux to the leading edge of the HPFTP blade, calculated as the product of h_c and the difference in temperature between the gas and the metal temperature (fig. 1), is shown in figure 19. The maximum heat flux in the HPFTP during engine start-up occurs during the second thermal transient and is approximately 22 800 kW/m^2. For comparison, the steady-state heat flux in the HPFTP to the leading edge near the blade tip is approximately 34 000 kW/m^2 based on a predicted gas-to-metal temperature difference of 88 °C (T(gas) = 840 °C) and h_c = 382 kW/m^2 K (67 392 Btu/hr ft^2 °F) (ref. 3). The heat flux during steady-state operation is almost 50 percent higher than that for the thermal transients which occur during engine start-up even though the steady-state gas temperature is significantly less than that during the first thermal transient.

The cause for the high steady-state heat flux is that the heat transfer coefficient is significantly increased as a result of the high gas pressures and high Reynolds numbers during steady-state engine operation.

The heat flux to the tube in the TSTR has also been calculated using the measured value of 27.5 kW/m^2 K for h_c (90° from stagnation), the gas temperature profile shown in figure 6(b) (dashed line), and the measured near-surface metal temperature shown in figure 12. The maximum heat flux to the tube in the TSTR was greater than 26 000 kW/m^2 as shown in figure 19. The value of 27.5 kW/m^2 K is a conservative estimate for h_c at the stagnation point; as previously discussed, the heat transfer coefficient at the stagnation point is probably somewhat greater than that measured at 90°. Even with the conservative value for h_c, it is significant to note that the maximum heat flux in the TSTR is greater than that in the HPFTP during the initial thermal transients which occur on engine start-up. However, it should be remembered that the heat flux during steady-state operation of the HPFTP exceeds both that in the TSTR and that during start-up of the HPFTP.

SUMMARY AND CONCLUSIONS

Gas temperatures and pressures were measured around the number two test position in the H_2/O_2 thermal shock test rocket located at NASA Lewis. Measured gas temperatures generally varied from 1210 to 1390 °C. Measured pressures were in good agreement with other studies for throat tubes in a square-chambered rocket engine. Heat transfer coefficients were determined at 90° and 180° from the stagnation point and resulted in values of 27.5 and 9.05 kW/m^2 K, respectively. Empirical predictions for h_c at the stagnation point were slightly greater than the values determined at 90° with a monotonic decrease from the stagnation point to 90°. Reducing the surface roughness of thermal barrier coated tubes by a factor of two did not have a significant effect on the heat transfer to the tubes.

A thermal model was developed to predict temperatures in a Mar-M246+Hf tube to verify the gas temperature and heat transfer measurements. Agreement between measured and predicted temperatures just below the surface of the Mar-M246+Hf tube was very good. The heat flux to this tube was also determined and showed a maximum value of 26 000 kW/m^2. The heat flux to the leading edge near the blade tip during start-up of the HPFTP was also calculated and showed a maximum of 22 800 kW/m^2 during the second thermal transient.

The results of this work indicate that the TSTR at NASA Lewis is capable of exceeding the heat flux during the thermal transients which occur on start-up of the HPFTP and that this test rocket engine provides a valuable tool for thermal shock testing of potential thermal barrier coatings and other proposed blade materials.

APPENDIX A

THERMAL CONDUCTIVITY AND VISCOSITY OF THE H_2-H_2O GAS MIXTURE AT 1174 AND 1338 °C

The thermal conductivity and viscosity of the H_2-H_2O gas mixture at 1174 and 1338 °C were calculated according to the semiemperical formulas given in reference 22. The thermal conductivity of the mixture is given as

$$k_{mix} = \sum_{i=1}^{2} \frac{x_i k_i}{\sum_{j=1}^{2} x_j \Phi_{ij}} \qquad 1,2 = H_2, H_2O \tag{A.1}$$

where x_i are the mole fractions of H_2 and H_2O and k_i are the thermal conductivities of the pure components. The coefficients Φ_{ij} are given as

$$\Phi_{ij} = \frac{1}{\sqrt{8}} \left(1 + \frac{M_i}{M_j}\right)^{-1/2} \left[1 + \left(\frac{\mu_i}{\mu_j}\right)^{1/2} \left(\frac{M_j}{M_i}\right)^{1/4}\right]^2 \qquad 1,2 = H_2, H_2O \tag{A.2}$$

where μ_i are the viscosities of pure H_2 and H_2O and M_i are the molecular weights.

The viscosity of the mixture is given as

$$\mu_{mix} = \sum_{i=1}^{2} \frac{x_i \mu_i}{\sum_{j=1}^{2} x_j \Phi_{ij}} \qquad 1,2 = H_2, H_2O \tag{A.3}$$

where the Φ_{ij} coefficients are given by equation (A.2). The mole fractions of H_2 and H_2O at 1174 and 1338 °C at 2.07 MPa were determined by calculations using the chemical equilibrium code described in reference 18 and are listed in table A.I. The thermal conductivities and viscosities of pure H_2 and H_2O were taken from references 13, 14, and 23 and are also given in table A.I. The thermal conductivities and viscosities of the gas mixture at 1174 and 1338 °C were calculated according to equations (A.1) to (A.3) and are also given in table A.I.

APPENDIX B

The thermal analysis model is capable of operating with temperature-dependent material and radiative properties. The temperature dependence of the thermal conductivity of Mar-M246+Hf is shown in figure B1(a) (ref. 21) and the temperature dependence of the heat capacity is shown in figure B1(b) (ref. 21). The emissivity for Ni-base alloys is strongly dependent on the surface condition of the specimen (ref. 15). The Mar-M246+Hf tube tested in this study exhibited a metallic luster prior to testing. A slight tarnish on the surface was evident after testing but the H_2-rich environment during the test, and the N_2 purge following the test minimized any significant oxide scale formation. Typical upper values for the emissivity of Ni-base alloys without thick oxide scales are shown in figure B2 (ref. 15). These values were input to the thermal model and the temperature of the surrounding chamber walls were assumed to be at 16 °C (60 °F) to evaluate the maximum radiative correction. The predicted temperatures at the surface and within the Mar-M246+Hf tube wall varied by less than 5 °C when radiative heat losses were taken into account.

REFERENCES

1. Carpenter, H.W.: Ceramic Turbine Elements. RI/RD84164, Rockwell International Co., Canoga Park, CA; NASA Contract No. NAS8-35327.

2. Abdul-Aziz, A.; Tong M.T.; and Kaufman, A.: Thermal-Finite-Element Analysis of Space Shuttle Main Engine Turbine Blade. NASA TM-100117, 1987.

3. Abdul-Aziz, A.: Private Communication. (This data was summarized in the publication given in reference 2.)

4. Holmes, R.R.: Vacuum Plasma Coatings for Turbine Blades. Advanced High Pressure O_2/H_2 Technology, S.F. Morea and S.T. Wu, eds., NASA CP-2372, 1985, pp. 74-90.

5. Nesbitt, J.A.: Thermal Modelling of Thermal Barrier Coatings in a High Heat Flux Rocket Engine, to be published.

6. Brindley W.J.; and Nesbitt, J.A.: Durability of Thermal Barrier Coatings in a High Heat Flux Environment. Advanced Earth-to-Orbit Propulsion Technology 1988, Vol. 1, R.T. Richmond and S.T. Wu, eds., NASA, Marshall Space Flight Center, 1988, pp. 661-674.

7. Lalos, G.T.: A Sonic-Flow Pyrometer for Measuring Gas Temperatures. J. Res. Nat. Bur. Stand., vol. 47, no. 3, Sept. 1951, pp. 179-190.

8. Terbush, R.K.: Improved Sonic Pyrometer. TEMPERATURE, Its Measurement and Control in Science and Industry, Vol. 3, C.M. Herzfeld, Editor-in-Chief, Part 2, Applied Methods and Instruments, A.I. Dahl, ed., Reinhold Publishing Corp., New York, 1962, pp. 595-600.

9. Talmor, E.: Heat Transfer to an Immersed Cylinder in Transonic Cross Flow. Chem. Eng. Prog., Symp. Ser., vol. 61, no. 59, 1965, pp. 50-56.

10. Talmor, E.: Heat Transfer to Small Diameter Throat Tubes. 56th National Meeting of the American Institute of Chemical Engineers, San Francisco, May 16-19, 1965.

11. High Temperature High Strength Nickel Base Alloys. International Nickel Inc., Saddle Brook, N.J., 1984.

12. SINDA - Systems Improved Numerical Differencing Analyzer. Available through Computer Software Management and Information Center (COSMIC), The University of Georgia, Athens, GA 30602, Program MSC 18597.

13. Kreith, F.: Principles of Heat Transfer, Second ed., International Textbook Co. Scranton, PA, 1965.

14. Thermophysical Properties of Matter. Vol. 1. Thermal Conductivity Metallic Elements and Alloys, Y.S. Touloukian, et al. eds., Plenum Press, 1970.

15. Thermophysical Properties of Matter. Vol. 7. Thermal Radiative Properties: Metallic Elements and Alloys, Y.S. Touloukian and D.P. DeWitt, eds., Plenum Press, 1970.

16. Elmore, D.L.; Robinson, W.W.; and Watkins, W.B.: Dynamic Gas Temperature Measurement System. NASA CR-168267-VOL-1 and NASA CR-168267, 1983.

17. Glawe, G.E.; Holanda, R.; and Krause, L.N.: Recovery and Radiation Corrections and Time Constants of Several Sizes of Shielded and Unshielded Thermocouple Probes for Measuring Temperature. NASA TP-1099, 1978.

18. Gordon, S.; and McBride, B.J.: Computer Program for Calculation of Complex Chemical Equilibrium Compositions, Rocket Performance, Incident and Reflected Shocks, and Chapman-Jouguet Detonations. NASA SP-273, 1976.

19. Talmor, E.: Turbulence Determination and Blockage Correction for Immersed Cylinder Heat Transfer at High Reynolds Numbers. A.I.Ch.E. J., vol. 12, no. 6, Nov. 1966, pp. 1092-1097.

20. Robinson, W.; and Han, L.S.: Experimental Investigation and Correlation of Point Heat Transfer From Cylinders in Various Arrangements to Air in Cross Flow. Proceedings of the Second Midwestern Conference on Fluid Mechanics, Ohio State University, Columbus, OH, 1952, pp. 349-361.

21. Chandler, W.T.: (RI/RD83-207, Rockwell International Corp., Canoga Park, CA; NASA Contract NAS3-23536) Materials for Advanced Rocket Engine Turbopump Blades. NASA CR-174729, 1983.

22. Bird, R.; Stewart W.; and Lightfoot, E.: Transport Phenomena. John Wiley and Sons, 1960, pp. 24, 258.

23. Svehla, R.A.: Estimated Viscosities and Thermal Conductivities of Gases at High Temperatures. NASA TR R-132, 1962.

24. Thermophysical Properties of Matter. Vol. 3. Thermal Conductivity; Nonmetallic Liquids and Gases, Y.S. Touloukian, P.E. Liley, and S.C. Saxena, eds., Plenum Press, 1970.

25. Thermophysical Properties of Matter. Vol. 11. Viscosity, Y.S. Touloukian, S.C. Saxena, and P. Hestermans, eds., Plenum Press, 1975.

TABLE I. - THERMOCOUPLE PROBE ASSEMBLIES

Probe number	Configuration[a]	Figure	Wire diameter, cm (in.)	Wire type	Dimensions, cm (in.)		
					X	Y	Z
1	BW-1	4(a)	0.0076 (0.003)	B	----------	0.10 (0.04)	0.076 (0.03)
2	BW-2	4(b)	.025 (.010)	B	0.127 (0.05)	.127 (.05)	.064 (.025)
3	↓	↓	.025 (.010)	R	.127 (.05)	↓ (↓)	.064 (.025)
4			.038 (.015)	B	.102 (.04)		.114 (.045)
5			.051 (.020)	R	.102 (.04)		.114 (.045)
6	WD	4(c)	.051 (.020)	R	----------	6.35 (2.5)	.51 (.2)
7	SWD	4(d)	.051 (.020)	R	.127 (.05)	6.35 (2.5)	.51 (.2)

[a]BW, butt-welded; WD, wedge; and SWD, shielded wedge.

TABLE II. - GAS PROPERTIES AND PARAMETERS FOR HEAT TRANSFER TO THE BUTT-WELDED THERMOCOUPLES

[D_1 = 0.0254 cm diameter wire; D_2 = 0.0508 cm diameter wire; Pr = Prandtl number = $C_p \mu/k_f$; Re = Reynolds number = $V D_i \rho/\mu$ (i = 1,2); Nu = Nusselt number = $h_c D_i/k_f$ (i = 1,2).]

(a) Gas properties (2.07 MPa)

Temperature, °C	C_p,[a] J/kg K	ρ,[a] kg/m^3	V,[a] m/sec	μ,[b] kg/m sec	k_f,[b] W/m K	Prandtl number
1173	7782	0.759	1896	0.0000372	0.490	0.591
1338	7364	.743	1906	.0000418	.527	.584

(b) Calculated parameters for heat transfer to the butt-welded thermocouples

Temperature, °C	Reynolds number		Nusselt number		h_c, W/m^2 K	
	D_1	D_2	D_1	D_2	D_1	D_2
1173	9800	19 600	51.0	78.2	98 310	75 450
1338	8600	17 200	47.0	72.1	97 590	74 920

[a]Reference 18.
[b]See appendix A.

TABLE III. - STAGNATION-POINT HEAT TRANSFER TO 0.9525 cm TUBES

Temperature, °C	Approach velocity, m/sec	Reynolds number	Blockage corrected Reynolds number
1173	388	75 300	135 600
1338	397	67 100	121 000

Tu, percent	Average Reynolds number[a]	$Nu/(Pr)^{1/3}$	Nu[b]	$h_{c,stag}$, W/m^2 K
0	128 000	400	480	25 524
11	128 000	570	680	36 368

[a]Average for 1173 and 1338 °C.
[b]Based on an average Pr of 0.586.

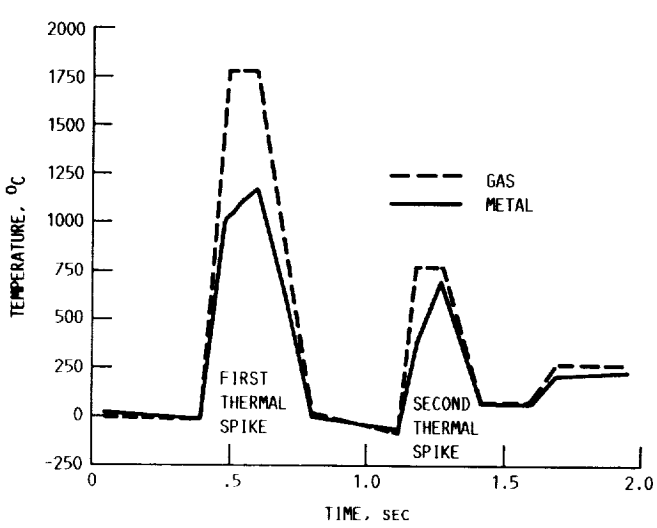

(a) GAS TEMPERATURE AND PREDICTED METAL TEMPERATURE (REF. 2,3).

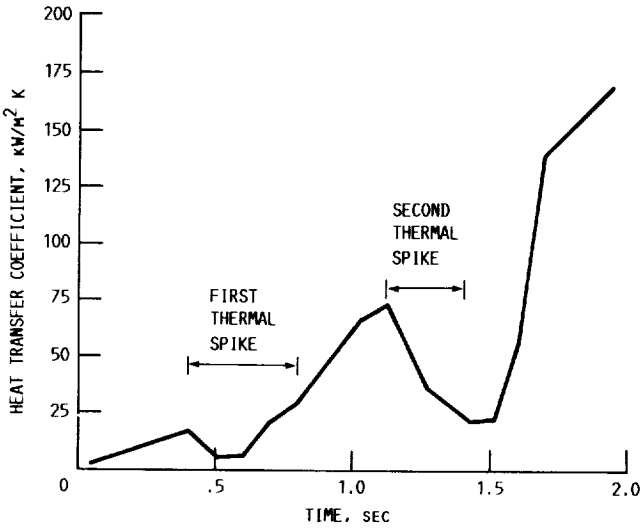

(b) HEAT TRANSFER COEFFICIENT (REF. 3).

FIGURE 1. - HEAT TRANSFER TO THE LEADING EDGE OF A FIRST STAGE TURBINE BLADE IN THE HPFTP DURING START-UP OF THE SSME.

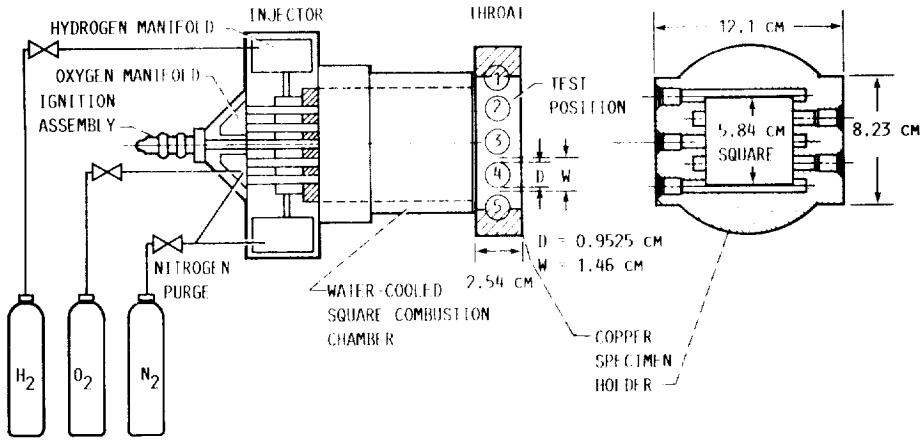

(a) SCHEMATIC VIEW OF THE ROCKET ENGINE AND COPPER SPECIMEN HOLDER.

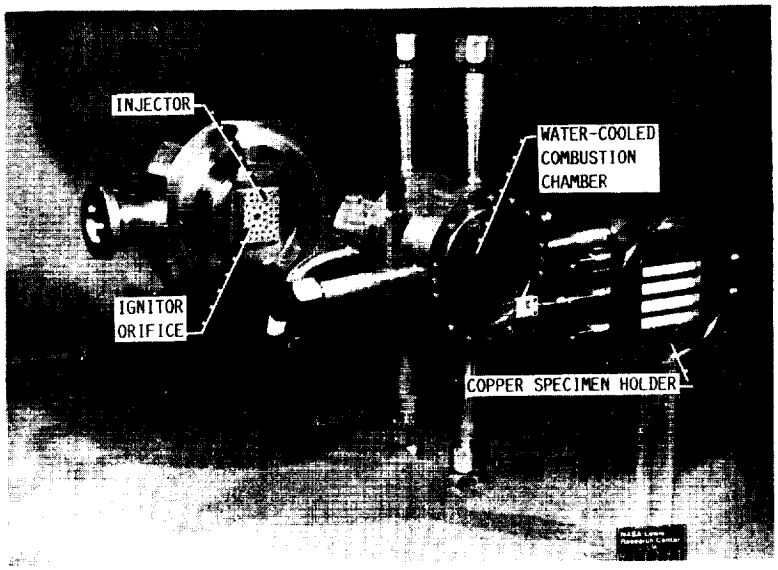

(b) VIEW OF THE OPERATING HARDWARE.

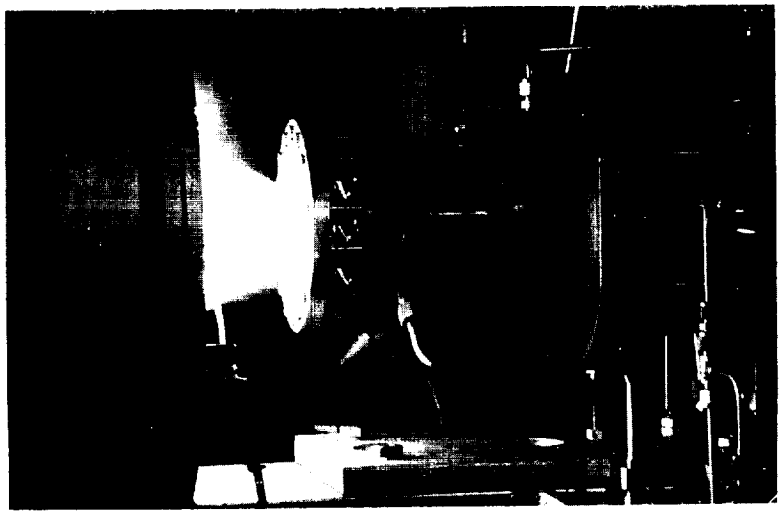

(c) VIEW OF THE ROCKET ENGINE WHILE FIRING.

FIGURE 2. - THERMAL SHOCK TEST ROCKET (TSTR) AT THE NASA LEWIS RESEARCH CENTER.

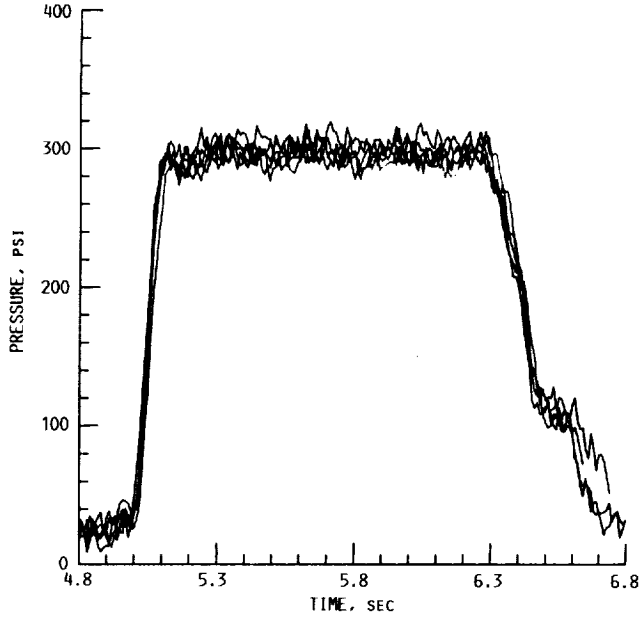

FIGURE 3. - CHAMBER PRESSURE DURING 1.3 SECOND TESTS MEASURED OVER A FIVE MONTH PERIOD.

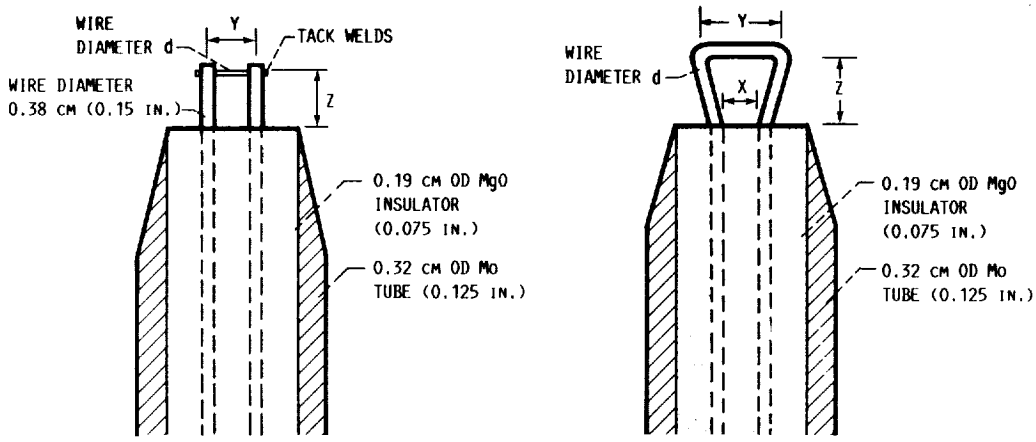

(a) AND (b) BUTT-WELDED.

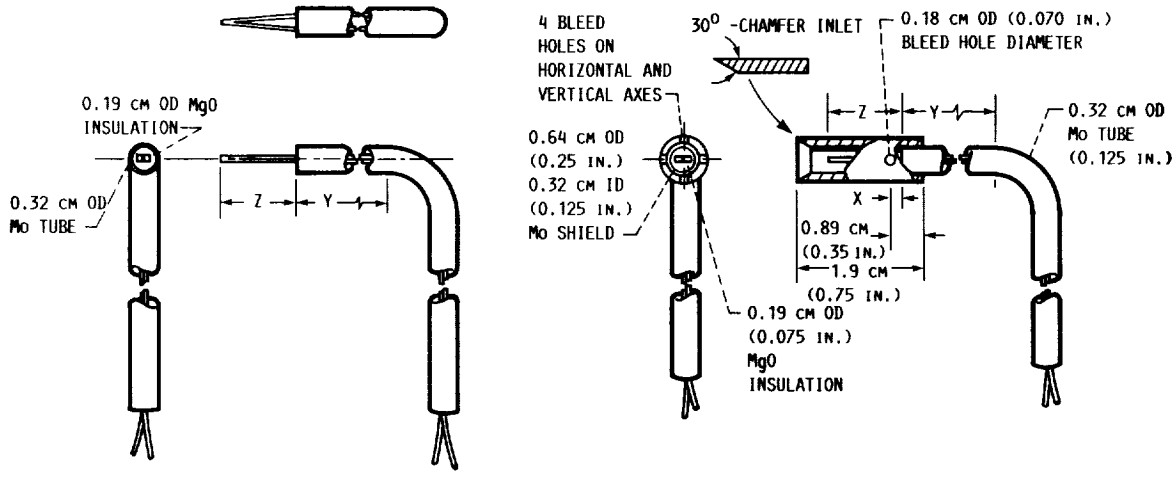

(c) WEDGE.

(d) SHIELDED WEDGE.

FIGURE 4. - SCHEMATIC VIEW OF THE THERMOCOUPLE PROBE ASSEMBLIES USED TO MEASURE GAS TEMPERATURES.

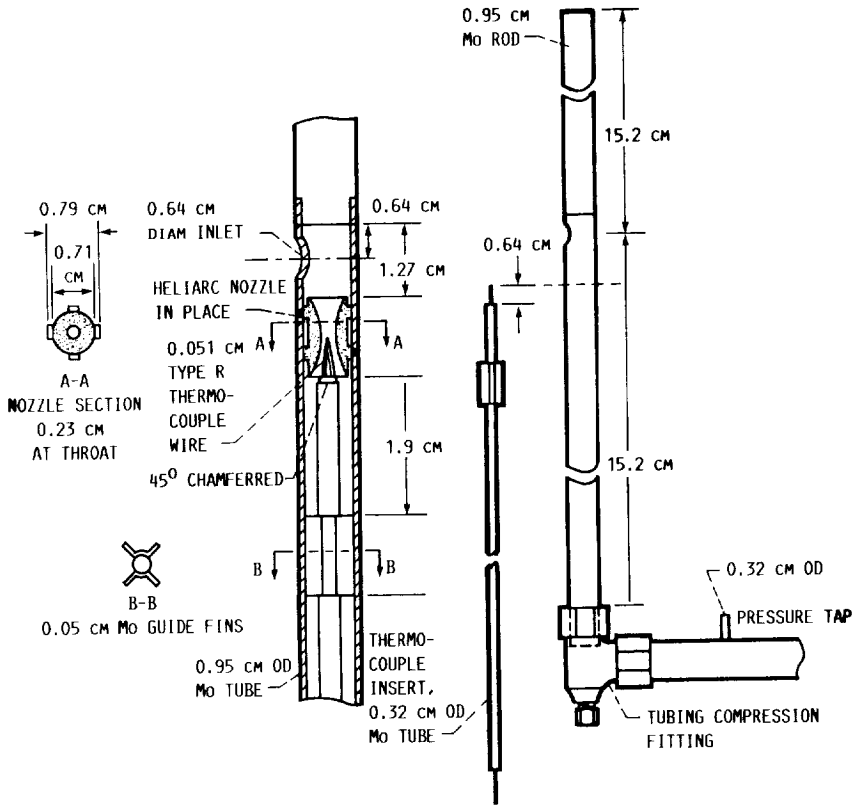

(e) SONIC ORIFICE PROBE.

FIGURE 4. - CONCLUDED.

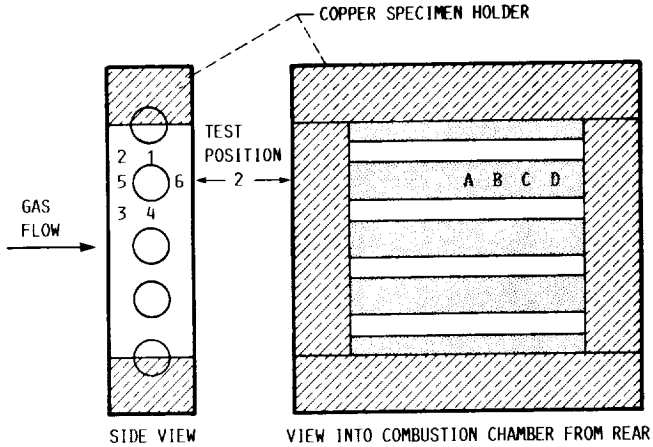

FIGURE 5. - THERMOCOUPLE POSITIONS AROUND THE TEST TUBE AND ALONG THE TUBE AXIS.

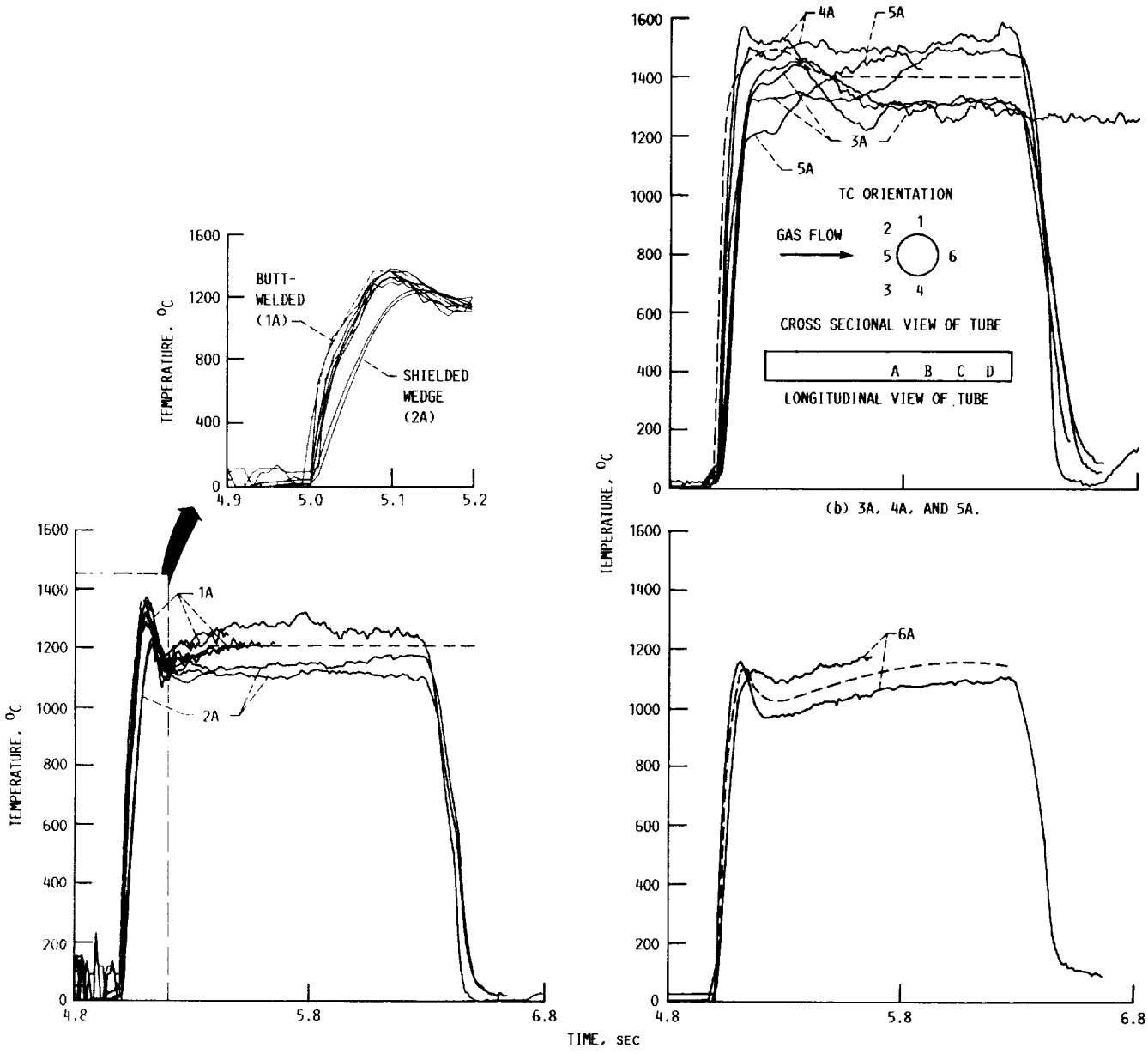

(a) 1A AND 2A.

(b) 3A, 4A, AND 5A.

(c) 6A.

FIGURE 6. - GAS TEMPERATURE MEASURED AT TC POSITIONS.

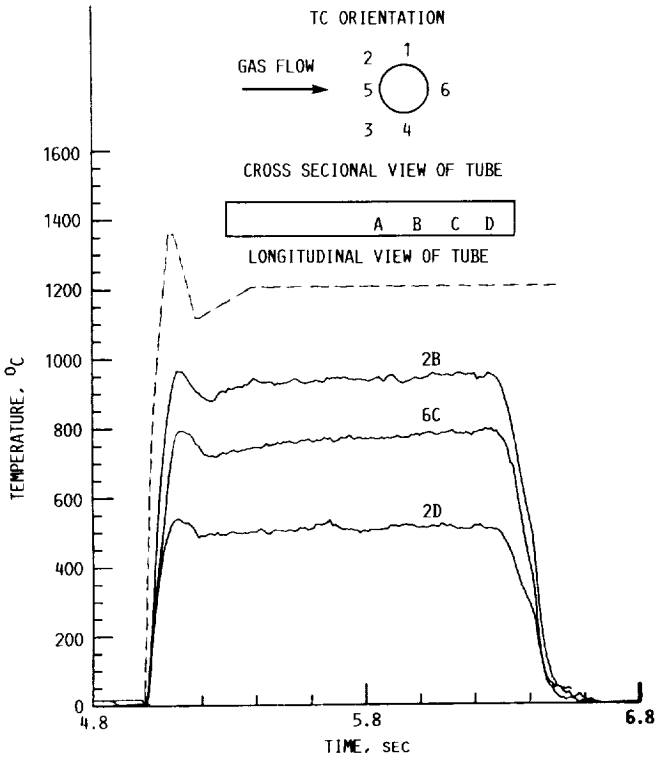

FIGURE 7. - GAS TEMPERATURES MEASURED AT TC POSITIONS 2B, 6C, AND 2D. REPRESENTATIVE TEMPERATURE FOR TC POSITION 1A (DASHED LINE) IS SHOWN FOR COMPARISON.

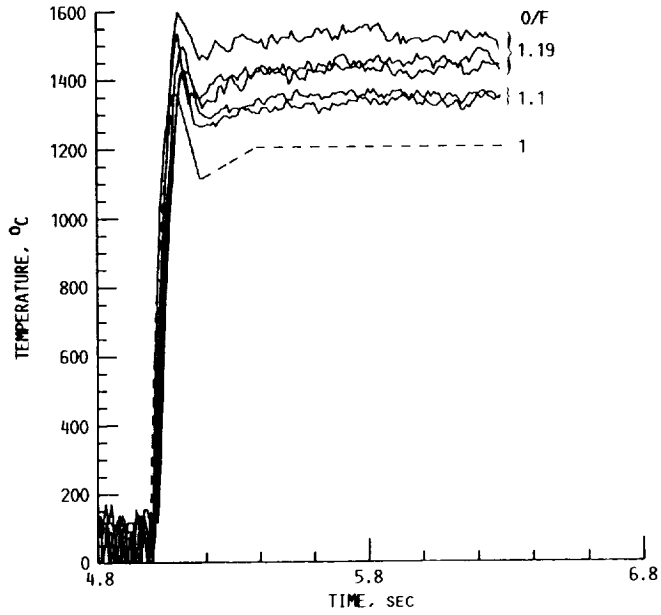

FIGURE 8. - GAS TEMPERATURES MEASURED AT TC POSITION 1A AT INDICATED O/F RATIOS OF 1.1 AND 1.19. REPRESENTATIVE TEMPERATURE FOR AN INDICATED O/F OF 1.0 (DASHED LINE) IS SHOWN FOR COMPARISON.

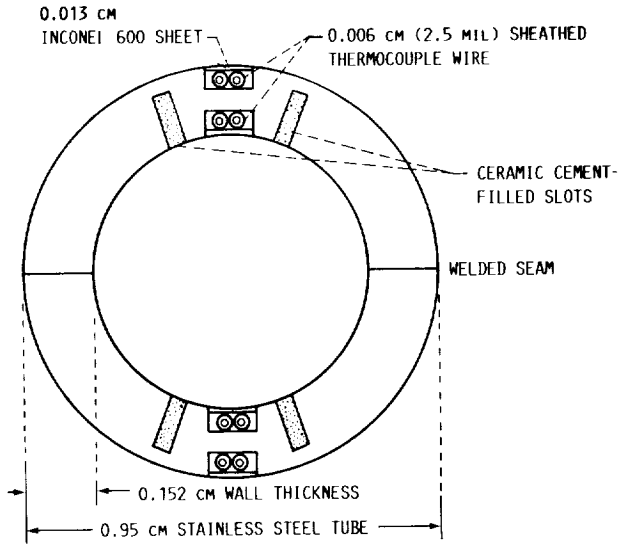

FIGURE 9. - SCHEMATIC CROSS SECTION OF THE WATER-COOLED, INSTRUMENTED STAINLESS STEEL TUBE USED FOR MEASURING HEAT TRANSFER COEFFICIENTS.

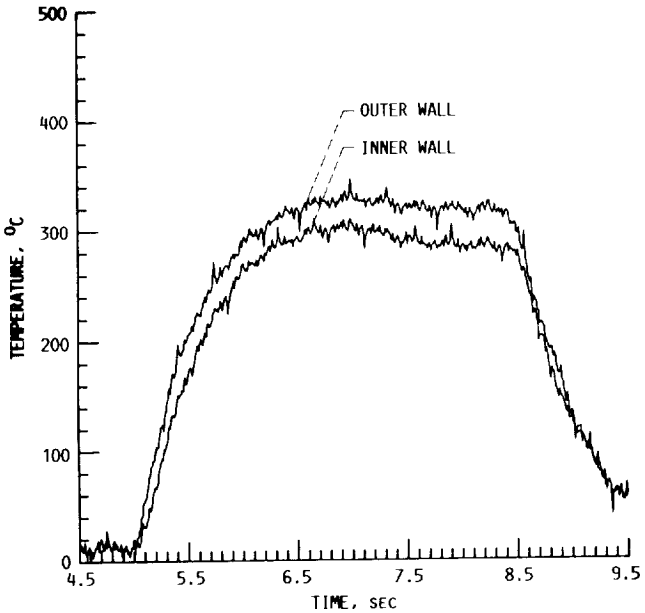

FIGURE 10. - MEASURED WALL TEMPERATURES IN THE WATER-COOLED STAINLESS STEEL TUBE 180° FROM THE STAGNATION POINT. (THE HIGHER TEMPERATURES ARE FOR THE OUTER WALL AND THE LOWER TEMPERATURES FOR THE INNER WALL.)

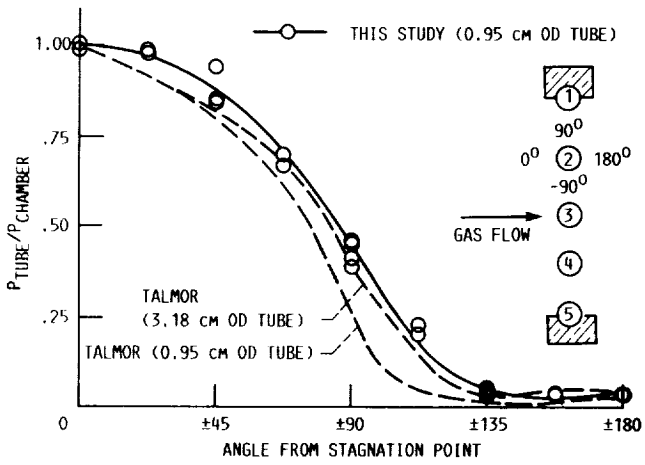

FIGURE 11. - ANGULAR DEPENDENCE OF THE NORMALIZED PRESSURE AROUND A TEST TUBE MEASURED IN THIS STUDY AND FOR OTHER THROAT TUBES IN A SQUARE-CHAMBERED ROCKET ENGINE (REF. 9,10).

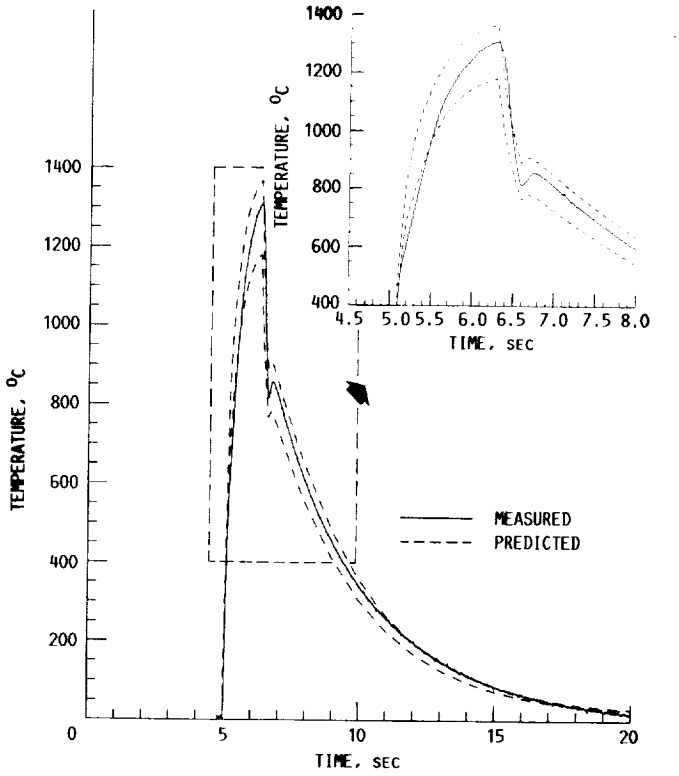

FIGURE 12. - MEASURED AND PREDICTED METAL TEMPERATURES AT THE STAGNATION POINT IN A BARE MAR-M246+Hf TUBE TESTED FOR 1.3 sec.

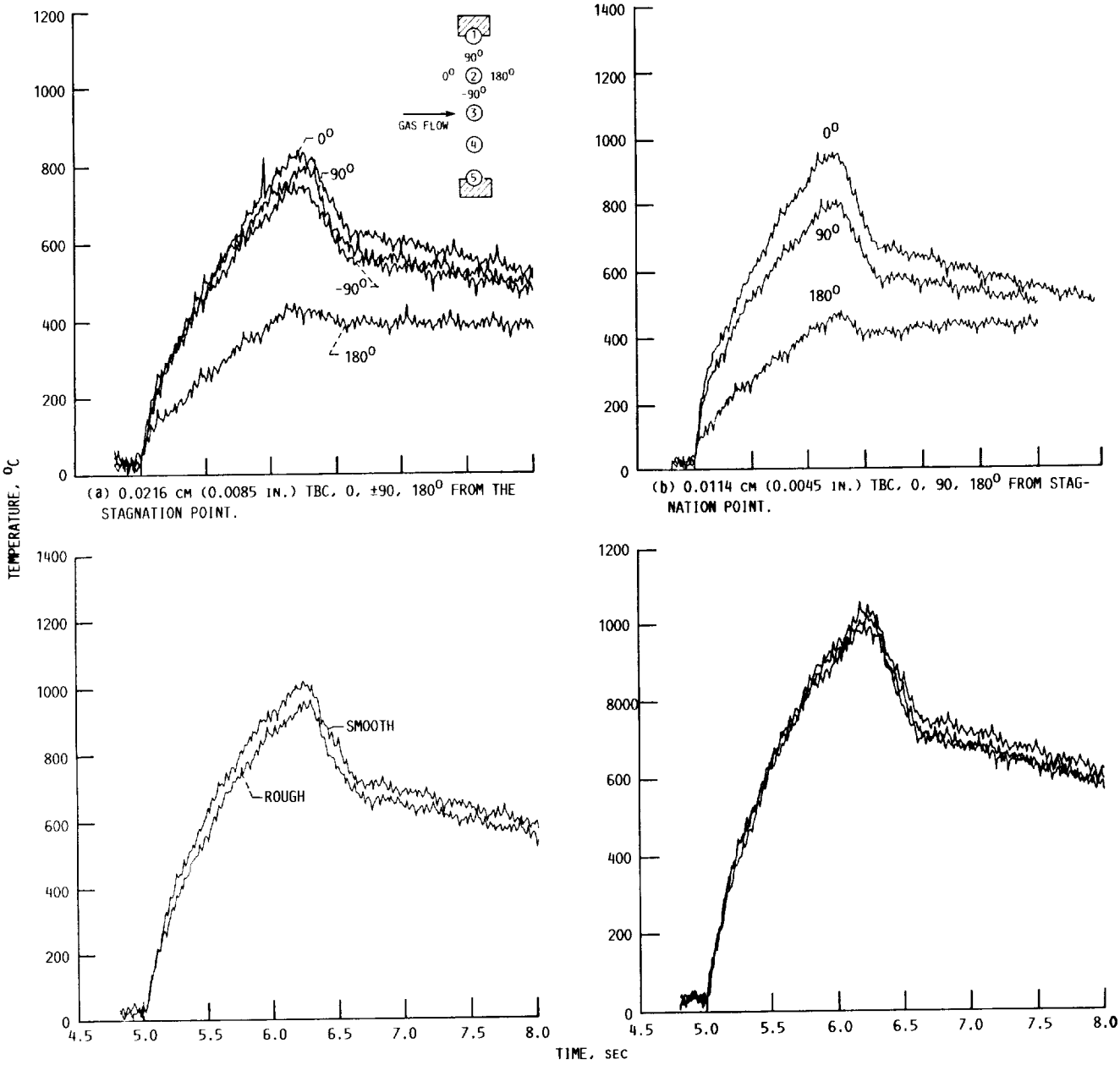

(a) 0.0216 cm (0.0085 in.) TBC, 0, ±90, 180° FROM THE STAGNATION POINT.

(b) 0.0114 cm (0.0045 in.) TBC, 0, 90, 180° FROM STAGNATION POINT.

(c) 0.0127 cm (0.005 in.) TBC 0° FROM THE STAGNATION POINT BEFORE AND AFTER SANDING.

(d) THE SAME COATING AS (c) AFTER SANDING MEASURED AT 0 AND ±45° FROM THE STAGNATION POINT.

FIGURE 13. - MEASURED NEAR-SURFACE METAL TEMPERATURES BELOW THERMAL BARRIER COATINGS TESTED AT AN INDICATED O/F = 1.

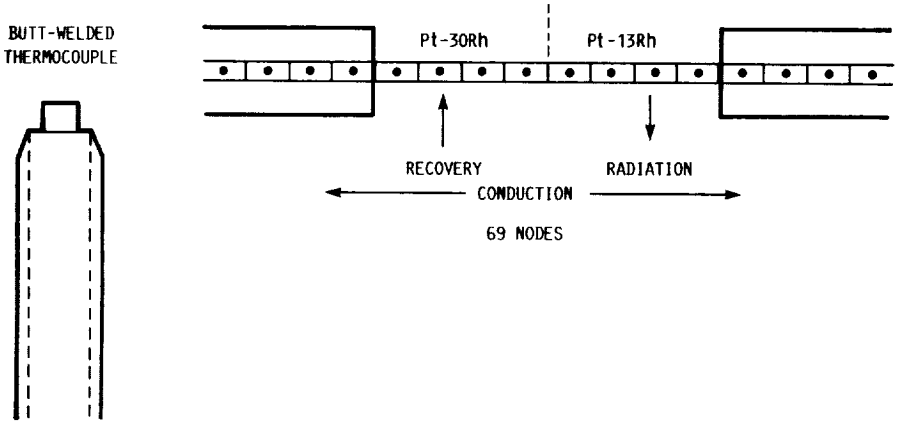

FIGURE 14. - THERMAL MODEL OF THE BUTT-WELDED THERMOCOUPLES.

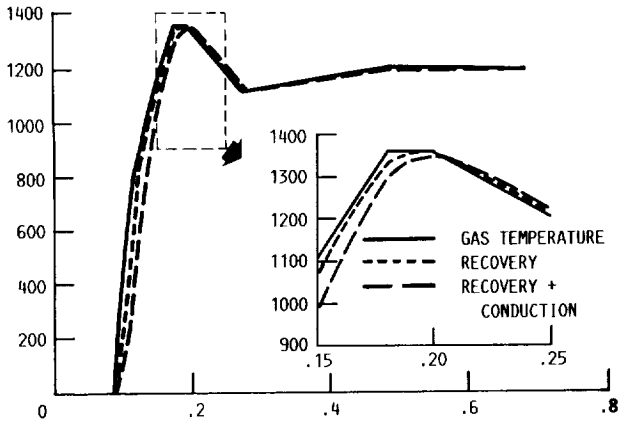

(a) SHOWING THE EFFECT OF RECOVERY AND CONDUCTION CORRECTIONS.

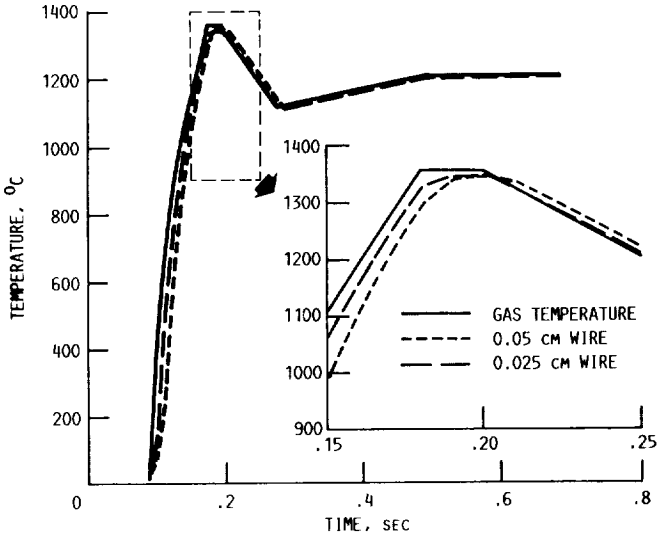

(b) SHOWING THE EFFECT OF TC WIRE DIAMETER ON THE THERMOCOUPLE RESPONSE.

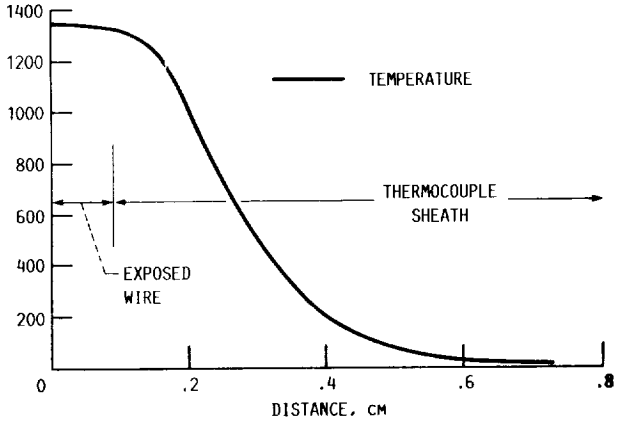

(c) SHOWING THE TEMPERATURE ALONG THE TC WIRE AT THE PEAK GAS TEMPERATURE.

FIGURE 15. - PREDICTED THERMOCOUPLE TEMPERATURES.

ORIGINAL PAGE
BLACK AND WHITE PHOTOGRAPH

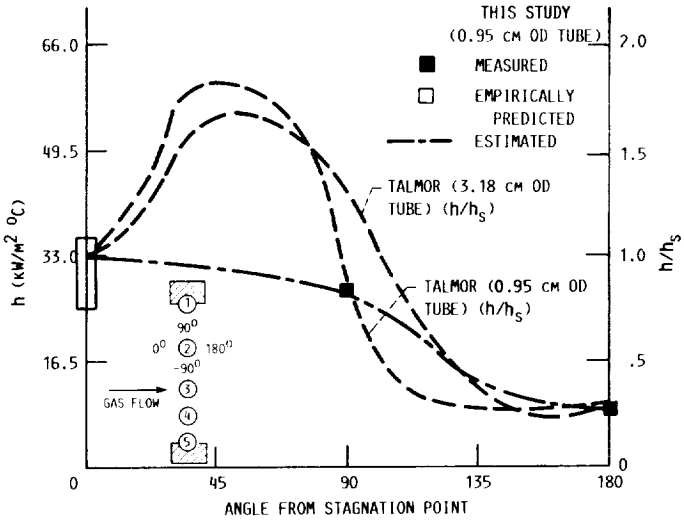

FIGURE 16. - MEASURED HEAT TRANSFER COEFFICIENTS (THIS STUDY) AND REPORTED (REF. 9,10) ANGULAR HEAT TRANSFER DISTRIBUTIONS.

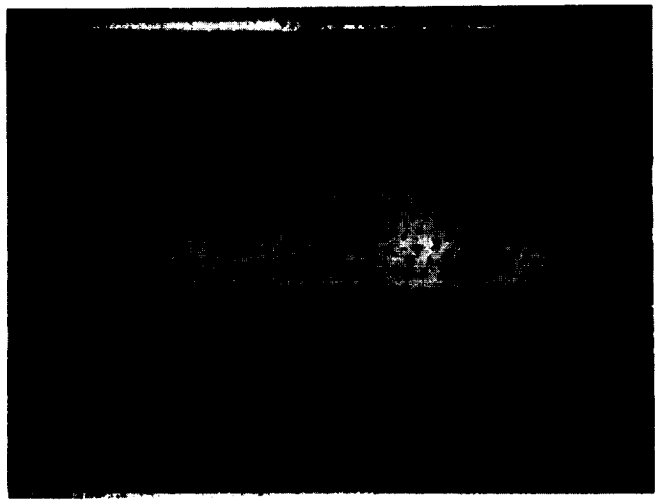

FIGURE 17. - EXHAUST SIDE OF SMOOTH CERAMIC-COATED TUBE SHOWING DARK DEPOSIT INDICATING REGION OF FLOW SEPARATION BETWEEN ±135° FROM THE STAGNATION POINT.

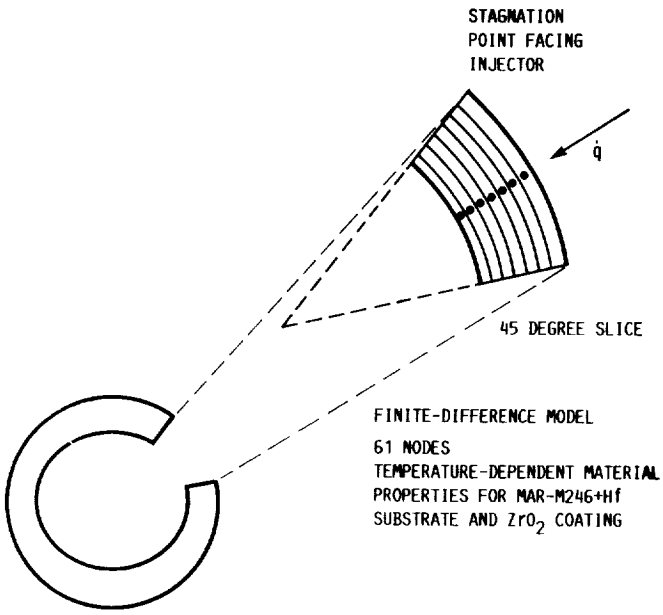

FIGURE 18. - THERMAL MODEL OF THE TEST TUBE.

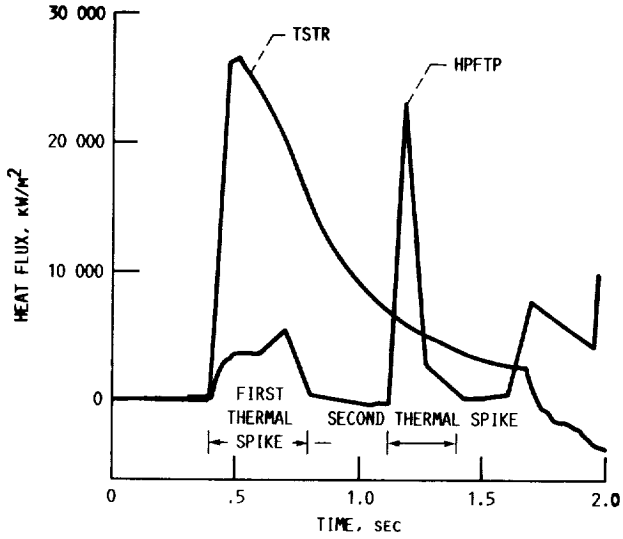

FIGURE 19. - COMPARISON OF THE HEAT FLUX IN THE THERMAL SHOCK TEST ROCKET AT NASA LeRC AND THAT PREDICTED FOR THE LEADING EDGE OF A BLADE IN THE HPFTP OF THE SPACE SHUTTLE MAIN ENGINE DURING ENGINE START-UP.

TABLE A.I. - THERMAL CONDUCTIVITY AND VISCOSITY OF THE H_2-H_2O GAS MIXTURE

Temperature, °C	x_{H_2}	x_{H_2O}	k_{H_2},[a] W/m K	k_{H_2O},[b] W/m K	k_{mix}, W/m K	μ_{H_2},[c] kg/m sec	μ_{H_2O},[d] kg/m sec	μ_{mix}, kg/m sec
1174	0.85	0.15	0.578	0.142	0.49	2.69×10^{-5}	5.04×10^{-5}	3.73×10^{-5}
1338	.825	.175	.637	.162	.528	2.90×10^{-5}	5.55×10^{-5}	4.18×10^{-5}

[a]Reference 24.
[b]Reference 13.
[c]Reference 25.
[d]Reference 23.

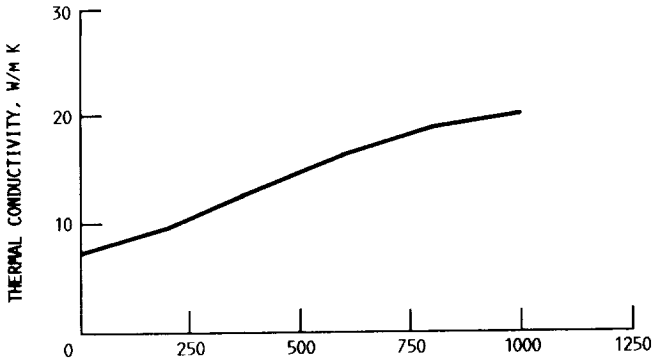

(a) THERMAL CONDUCTIVITY.

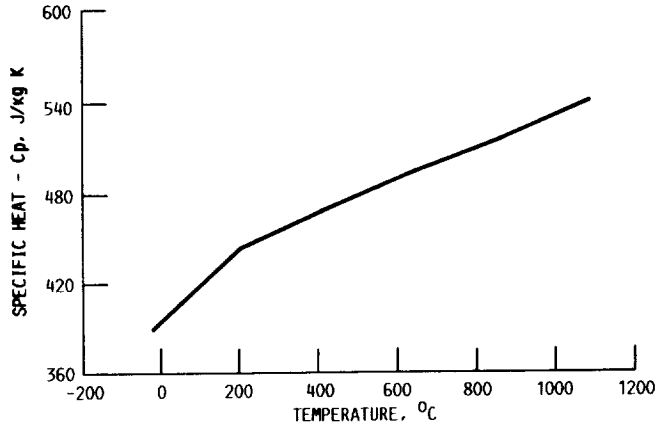

(b) SPECIFIC HEAT.

FIGURE B1. - THERMOPHYSICAL PROPERTIES FOR MAR-M246+Hf (REF. 21).

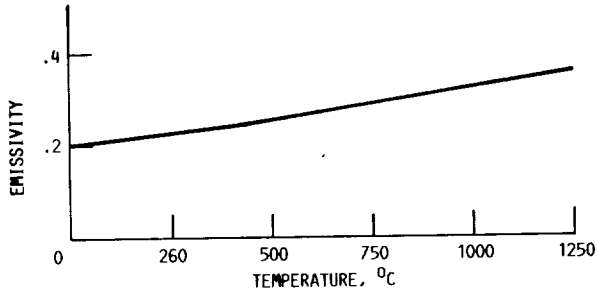

FIGURE B2. - APPROXIMATE TEMPERATURE DEPENDENCE OF THE EMISSIVITY FOR NI-BASE ALLOYS.

NASA
National Aeronautics and Space Administration

Report Documentation Page

1. Report No.	2. Government Accession No.	3. Recipient's Catalog No.
NASA TM-102336		

4. Title and Subtitle	5. Report Date
Heat Transfer to Throat Tubes in a Square-Chambered Rocket Engine at the NASA Lewis Research Center	October 1989
	6. Performing Organization Code

7. Author(s)	8. Performing Organization Report No.
James A. Nesbitt and William J. Brindley	E-5045
	10. Work Unit No. 505-63-1A

9. Performing Organization Name and Address	11. Contract or Grant No.
National Aeronautics and Space Administration Lewis Research Center Cleveland, Ohio 44135-3191	
	13. Type of Report and Period Covered Technical Memorandum

12. Sponsoring Agency Name and Address	14. Sponsoring Agency Code
National Aeronautics and Space Administration Washington, D.C. 20546-0001	

15. Supplementary Notes

16. Abstract

A gaseous H_2/O_2 rocket engine was constructed at the NASA Lewis Research Center to provide a high heat flux source representative of the heat flux to the blades in the high-pressure fuel turbopump (HPFTP) during startup of the space shuttle main engines. The high heat flux source was required to evaluate the durability of thermal barrier coatings being investigated for use on these blades. The purpose of the present work was to evaluate the heat transfer, and specifically, the heat flux to tubes located at the throat of the test rocket engine and to compare this heat flux with the heat flux to the blades in the HPFTP during engine startup. This purpose was accomplished by measuring gas temperatures, pressures and heat transfer coefficients in the test rocket engine. Near-surface metal temperatures below thin thermal barrier coatings were also measured at various angular orientations around the throat tube to indicate the angular dependence of the heat transfer coefficients. A finite-difference model for a throat tube was developed and a thermal analysis was performed using the measured gas temperatures and the derived heat transfer coefficients to predict metal temperatures in the tube. Near-surface metal temperatures of an uncoated throat tube were measured at the stagnation point and showed good agreement with temperatures predicted by the thermal model. The maximum heat flux to the throat tube was calculated and compared to that predicted for the leading edge of an HPFTP blade. It is shown that the heat flux to an uncooled throat tube is slightly greater than the heat flux to an HPFTP blade during engine startup.

17. Key Words (Suggested by Author(s))	18. Distribution Statement
Heat transfer; Throat tubes; Heat transfer coefficients; Thermal modelling; Rocket engine; Heat flux; SSME-HPFTP	Unclassified – Unlimited Subject Category 20

19. Security Classif. (of this report)	20. Security Classif. (of this page)	21. No of pages	22. Price*
Unclassified	Unclassified	32	A03

NASA FORM 1626 OCT 86

*For sale by the National Technical Information Service, Springfield, Virginia 22161